An Experimental Study of X-Band Synthetic Aperture Radar (SAR) Imagery for Marine Oil Slick Monitoring

Stine Skrunes[1], Camilla Brekke[1], Torbjørn Eltoft[1] and Véronique Miegebielle[2]

[1]Department of Physics and Technology, University of Tromsø, Tromsø, Norway

[2]Total S. A., C. S. T. J. F., Pau Cedex, France

stine.skrunes@uit.no

Abstract

In this study, the usefulness of multi-polarization X-band SAR data for oil slick monitoring is investigated. The effect of incidence angles and noise contamination, and the combination of HH and VV polarization channels for oil slick monitoring is discussed. Dual-polarization data collected by TerraSAR-X and COSMO-SkyMed during two large-scale oil spill exercises in the North Sea is analysed. Oil slicks are detected in low wind speeds (1.6-5 m/s) over a range of incidence angles. While the noise contamination of the signal is seen to increase with increasing incidence angles, the multi-polarization features provide less information at the lowest incidence angles here available (~20°-21° for TerraSAR-X and ~24°-26° for COSMO-SkyMed). When slick characterization utilizing multi-polarization features is desired, intermediate incidence angles seem preferable. For TerraSAR-X data at incidence angles ~27°-29° and ~ 41°-42°, consistency in feature values between scenes is seen to some extent. No clear variations with slick age are observed. TerraSAR-X data, being coherent in phase, is found more useful for multi-polarization analysis than COSMO-SkyMed in this data set.

1   Introduction

Synthetic Aperture Radar (SAR) has proven itself to be a valuable tool for detection and monitoring of marine oil spills. Still, more research on the influence of sensor parameters such as frequency, incidence angle and polarization on the oil spill detection ability are requested to enable more reliable oil spill detection services.

Oil spills are detected in SAR imagery as areas of reduced backscatter compared to the surrounding clean sea. The presence of oil can decrease the backscatter power in two ways, i.e. by reducing the surface roughness and by reducing the effective dielectric constant of the surface (Minchew, 2012). Limitations for oil spill observation by SAR sensors are the restricted wind speed range in which detection is possible, the problem of look-alikes, and limitations related to sensor parameters. According to Girard-Ardhuin et al., 2005, efficient detection at C-band frequency requires wind speeds in the range 2-3 m/s to 10-14 m/s. Lower wind speeds may not provide enough contrast in surface roughness, while stronger winds may mix the oil into the subsurface waters. Look-alike phenomena are natural phenomena, which produce similar SAR signatures as oil spills and can cause false detections. This includes e.g. natural biogenic slicks produced by marine organisms, low wind areas (< 3m/s) and grease ice (Brekke and Solberg, 2005).

SAR sensors are generally considered independent of light and weather conditions. However, heavy rain may attenuate the signals, especially at higher frequencies. Hence X-band is more prone to this than C-band (Danklmayer et al., 2009). In addition to environmental conditions, oil spill detection and characterization by SAR is affected by oil slick properties, e.g. thickness, chemical composition and age. The oil's physical and chemical properties will change with time due to weathering processes, including evaporation, emulsification, dissolution and

oxidation. Also sensor parameters such as frequency, incidence angle, resolution, noise floor and polarization are key factors affecting the imaging of slicks. In general, co-polarization channels, preferably VV, are used for oil spill observation. Depending on wind and radar frequency, incidence angles in the range 20° to 45° have been suggested the most suitable (Girard-Ardhuin et al., 2005). Over the last decades, mostly C-band SAR sensors have been used for satellite based oil spill detection and monitoring. However, poor temporal coverage of individual satellites composes a limitation for operational oil spill detection services. Two of the more recently launched satellites, TerraSAR-X and COSMO-SkyMed, as well as planned missions such as KOMPSat-5, operate in the X-band frequency range. Exploitation of these sensors for oil spill purposes may enhance the temporal coverage and improve satellite based oil spill detection services. X-band SAR sensors are used for oil spill detection in e.g. Gade et al., 1998, Ivanov, 2010, Kim et al., 2010, Vespe et al., 2011 and Del Frate et al., 2011. Note that single-polarization data sets are investigated in these studies. By combining several polarization channels, features related to physical properties and scattering behaviour of the observed target surface can be extracted. Multi-polarization techniques seem promising for oil versus look-alike discrimination and for extraction of slick properties, as discussed by e.g. Migliaccio et al., 2007, Migliaccio et al., 2009a, Migliaccio et al., 2009b, Minchew et al., 2012, Nunziata et al., 2008, Skrunes et al., 2012, Tian et al., 2010, Velotto et al., 2011 and Zhang et al., 2011. Most of these studies are performed on C- and L-band SAR data.

This study aims to investigate the capability of multi-polarization SAR sensors in the X-band frequency range for oil slick monitoring. Dual-polarization (HH, VV) SAR data collected by TerraSAR-X and COSMO-SkyMed during two large-scale oil spill exercises in the North Sea is analysed. The key points of this paper are, a) to relate the noise properties and visual slick-to-sea contrast of multi-polarization features to the range of incidence angles, and b) to give a preliminary comparison of different slick types, slicks of different ages, temporal changes of specific slicks and feature value consistency between scenes.

Slicks were detected by both COSMO-SkyMed and TerraSAR-X in low wind conditions over a range of incidence angles. The multi-polarization features seem to give less information in the scenes at the lowest incidence angles, while the noise contamination problem increases at larger incidence angles. Hence, for this data set, medium range incidence angles seem optimal. COSMO-SkyMed dual-polarization data is not coherent in phase, and only intensity based multi-polarization features are extracted based on these scenes. The intensity based features here provide lower slick-to-sea contrast compared to features including phase information, making the COSMO-SkyMed data less useful for multi-polarization analysis than TerraSAR-X. For TerraSAR-X data at incidence angles ~27°-29° and ~ 41°-42°, the features including phase clearly distinguish slicks from surrounding sea, and consistency in feature values between the scenes are seen to some extent. No clear variations with slick ages are found. Some visual difference between a biogenic slick and mineral oil slicks are observed.

Section 2 describes the data set and a data quality analysis is given in Section 3. Section 4 presents a multi-polarization analysis, while Section 5 concludes the paper.

2   Experimental Setup and Data Collection

Oil-on-water exercises were conducted by the Norwegian Clean Seas Association for Operating Companies (NOFO) in June 2011 and June 2012. Oil was released onto the sea surface for the purpose of procedure and equipment testing. The X-band satellite SAR data acquired during the exercises are discussed in this study.

During the 2011 exercise, three substances were released, i.e. oil emulsion, crude oil and plant oil. The emulsion and crude oil slicks were subjected to mechanical recovery and chemical dispersion respectively, while the plant oil was left on the surface untouched. In the 2012 exercise, four releases of oil emulsion were done, in addition to release of plant oil and oleyl alcohol (OLA). Mechanical recovery and dispersion were applied to the emulsion slicks, while the plant oil and OLA were left undisturbed. In both exercises, the plant oil and OLA were used for simulation of natural slicks/look-alikes (Skrunes et al., 2012).

Table 1 gives an overview of the data set collected by X-band SAR sensors. All TerraSAR-X scenes are dual-pol (HH, VV) Stripmap scenes, and all COSMO-SkyMed scenes are dual-pol (HH, VV) Stripmap PingPong scenes. Intensity images are shown in Fig. 1 and Fig. 2 for TerraSAR-X and COSMO-SkyMed respectively. The yellow boxes indicate selected areas within the different regions used in the analysis.

The first TerraSAR-X scene in Fig. 1 (TSX2011a) contains an emulsion slick, which has been on the surface for ~18 hours at the time of satellite acquisition. The same slick is also imaged in the second scene (middle slick in TSX2011b), which is acquired about 29 hours after emulsion release. This scene also contains plant oil (left) and crude oil (right), imaged respectively about 13 and 9 hours after release.

The first TerraSAR-X scene from 2012 (TSX2012a) does not contain any visible slicks, even though several oil releases are within the coverage area. The slick positions are close to the group of ships seen as bright point targets. The backscatter from ocean areas is known to decrease with increasing incidence angle (Hoogeboom and Lidicky, 2008), and we suspect the incidence angles of this scene, 55.4° - 56.0°, are too large for detection of slicks. The last TerraSAR-X scene in Fig. 1 (TSX2012b) contains three emulsion releases, with slick ages of ~28.5, ~25 and ~12 hours.

The first COSMO-SkyMed scene in Fig. 2 (CSM2012a) contains the plant oil slick, ~2 hours old, and several emulsion slicks released ~9.5, ~5 and ~1.5 hours before the satellite pass. The second scene (CSM2012b) contains the same slicks as CSM2012a, with slick ages of about 13.5 hours for the plant oil and about 21, 16.5 and 13 hours for the emulsion slicks. The last COSMO-SkyMed scene (CSM2012c) shows the same emulsion slicks as TSX2012b, here with ages ~34.5, 30, 26.5 and ~13.5 hours.

3   Data Quality

The noise equivalent sigma zero (NESZ) describes the strength of the additive system noise in a sensor. When working with low-backscatter areas such as oil-covered sea surfaces, a signal-to-noise analysis, comparing the signal level to the NESZ, should be considered. This is especially important if oil slick *characterization* is of interest, in addition to slick *detection*. If the NESZ exceeds the signal levels, information is lost in the noise. Noise levels and variations with incidence angles for the scenes investigated here are discussed next.

3.1   TerraSAR-X

The NESZ for TerraSAR-X lies between -19 dB and -26 dB, depending on the incidence angles, with an average of -21 dB (Fritz and Eineder, 2010). Fig. 3 presents signal-to-noise analyses for the TerraSAR-X scenes described in Table 1, comparing the NESZ of each scene to the signal levels. Each vertical bar shows the mean and standard deviation of backscatter values (σ_0) computed within the boxes of 50×50 pixels shown in yellow in Fig. 1. The sensor noise floor is plotted as function of incidence angle. In general, it is seen that the VV channel provides

larger backscatter values than the HH channel. The difference is small at low incidence angles (TSX2011b) and larger at higher incidence angles (TSX2011a and TSX2012b). This is a well-known behaviour for backscattering over sea surfaces (Hoogeboom and Lidicky, 2008). For the three scenes with incidence angles below ~ 42°, the NESZ lies between -20 dB and -25 dB, while the last scene has a NESZ about -18 to -19 dB. At the lowest incidence angles, in TSX2011b, all mean values are above the noise floor, and only the bar of the crude oil slightly crosses the NESZ. In TSX2011a and TSX2012b, the slick-covered areas have mean signal values close to and slightly below the noise floor. Also the clean sea signal values approach the noise floor as the incidence angles increase. In TSX2012a, at 55.6°-56°, even the mean clean sea signal lies on or below the noise floor. From this, the incidence angle seems to be an important factor influencing the amount of noise contamination of the SAR signal, and the largest incidence angles should be avoided. In this context we should keep in mind that the backscatter levels are also affected by wind speed, and the ocean backscatter is known to increase with wind speed as described in e.g. Kim et al., 2010. The low wind speeds at the time of these acquisitions (1.6 – 4 m/s for scenes including slicks) could decrease the signal-to-noise ratio (SNR).

3.2   COSMO-SkyMed

Agenzia Spaziale Italiana (ASI) provides a total NESZ ≤ -19 dB for all COSMO-SkyMed products (Italian Space Agency, 2009). At delivery, a noise removal, where a noise estimate is subtracted from each pixel, has been applied to the data. Where the difference is negative, i.e. where the noise estimate exceeds the signal, the pixel value is set to zero. In the first two COSMO-SkyMed scenes, a high percentage of the pixel values (62.5% for HH and 49.4% for VV in CSM2012a, and 71.1% for HH and 61.9% for VV in CSM2012b) were found to be zero. From Table 1, it can be seen that the incidence angles of these scenes are in the range 41.7° - 43.2° and 39.6° - 41.7°. The last COSMO-SkyMed scene has incidence angles between 23.5° and 26.1°, and contains only 3.4% zero-values in each polarization channel. Hence, the incidence angle seems to be important for the level of noise contamination also for COSMO-SkyMed.

4   Multi-Polarization Analysis

Dual- and quad-polarization SAR systems measure two or four transmit-receive polarization combinations, providing more data for characterization of the observed target surface. By combining the different channels, information related to physical properties and scattering behaviour of the surface can be extracted. Multi-polarization analysis may improve the ability to do oil slick characterization, including oil versus look-alike discrimination and extraction of slick information. A multi-polarization (HH, VV) analysis is here applied to the six scenes containing visible slicks.

4.1   Multi-Polarization Features

Definitions of the five multi-polarization features investigated in this study are defined in Table 2. The *real part of co-polarization correlation*, the *standard deviation of co-polarized phase difference*, the *co-polarization power ratio* and the *entropy* have previously been applied and found useful for oil slick characterization (Migliaccio et al., 2007; Migliaccio et al., 2009a; Migliaccio et al., 2009b; Minchew et al., 2012; Nunziata et al., 2008; Tian et al., 2010; Velotto et al., 2011; Zhang et al., 2011). It should be noted that in this study, we are only utilizing the co-polarization measurements. This means that the covariance matrix only has two eigenvectors, and the entropy will hence deviate some from the traditional definition (Cloude and Pottier,

1997) where also the cross-polarization channels are included. All features are here computed using a 9×9 pixels sliding window.

In the case of COSMO-SkyMed PingPong mode, based on alternating polarizations between bursts, the coherence between the polarimetric channels is not preserved (Nunziata and Migliaccio, 2013). Only the two intensity-based features in Table 2, i.e. the co-polarization power ratio and the *normalized co-polarization difference,* are hence computed from the COSMO-SkyMed scenes. These two features are presented in Fig. 4 and Fig. 5 for TerraSAR-X and COSMO-SkyMed respectively. In the co-polarization power ratio, some of the emulsion in TSX2011a and a few pixels related to the crude oil in TSX2011b may be discerned from the surrounding sea, while the slicks can be more clearly identified in TSX2012b. In CSM2012a and CSM2012b, the slick regions may be recognized, but with very poor contrast to the sea. For CSM2012c, the slicks are not visible at all in this feature. HH and VV backscatter is expected to be very similar for ocean surfaces at low incidence angles, with increasing difference between the two as the incidence angle increases. This can explain why the scenes at the largest incidence angles show the slicks more clearly. The co-polarization power ratio may hence be useful only at larger incidence angles. Similar results as for co-polarization power ratio are seen for the normalized co-polarization difference, but with slightly improved contrast.

In the case of TerraSAR-X, the acquisition method gives coherent polarization channels, where also the phase information may be used in data interpretation. The first three features in Table 2 are computed based on both intensity and phase information and results are presented in Fig. 6. A less noisy result and better slick-to-sea contrasts are observed in these features, compared to the intensity-based features in Fig. 4. The best visual contrasts are found in the entropy and standard deviation of co-polarized phase difference. TSX2011a and TSX2012b provide the best visual results, possibly due to the larger incidence angles. As seen in Fig. 3, the mean slick signals are closer to the noise floor in these two scenes, i.e. we are here partly comparing the features of ocean signal to noise statistics.

Slick characterization, including discrimination between oil slicks and natural look-alikes, and extraction of slick information, is desired for operational purposes. A few observations regarding slick characterization may be done in relation to Fig. 6. In the 2011 data set, the emulsion slick is imaged twice, in TSX2011a and in TSX2011b (middle slick). In the second acquisition, the slick has become smaller and more fragmented. Lower entropy values, larger correlation and lower standard deviation of co-polarized phase difference are observed in the slick in TSX2011b, i.e. a behaviour more similar to clean sea is found here. As also the sea surface show similar variations in feature values between the two scenes, the difference in sensor parameters or environmental conditions may cause the variations between scenes, rather than the difference in slick age.

All three slicks in TSX2012b are produced by the same type of emulsion, but released at different times. No visual difference between the slicks can be related to slick ages. In TSX2011b, three slicks, produced by chemically different substances, are present. The plant oil simulates a natural biogenic look-alike slick, and forms a different type of film on the sea surface (Skrunes et al., 2012) compared to the crude oil and oil emulsion. Some visual difference between the look-alike and the two mineral oil slicks can be observed in the multi-polarization features, possibly due to difference in scattering mechanisms.

To further evaluate the slick discrimination potential and variations between scenes, feature value distributions are discussed next.

4.2   Feature Distributions

To which extent the multi-polarization features discriminate between different areas in the images, and how much the feature values deviates between different scenes, are important questions. This is investigated for the three TerraSAR-X scenes with visible slicks, for the four most promising features discussed in the previous section. Fig. 7 presents histograms of the feature values of the real part of co-polarization correlation, the entropy, the standard deviation of co-polarized phase difference and the normalized co-polarization difference. The histograms are computed based on the regions of 50×50 pixels indicated by yellow boxes in Fig. 1. Different aspects of Fig. 7 are here discussed:

- Slick detection, i.e. discriminating clean sea (blue) from slick-covered areas:
  There is some overlap between the slicks and the sea in each individual scene. The normalized co-polarization difference does not discriminate between the slicks and the sea, while the distributions are better separated in the other three features. The additional information contained in the phase may explain the improved separation here. The best distinction between slicks and sea seems to be provided by the real part of the co-polarization correlation.

- Slick characterization, i.e. discrimination between oil slicks and look-alikes:
  When comparing the plant oil (green) to the mineral oils present in the same scene, i.e. the continuous black and red lines, a relatively high degree of overlap is observed. The lowest amount of overlap is found in the three features including the phase information. In these features, the plant oil is quite well separated from the emulsion slicks of the other two scenes.

- Feature value consistency between scenes:
  Knowledge about consistency in feature values from scene to scene, and the possible dependency on varying sensor, environment and slick parameters, is important if multi-polarization features are to be used operationally. From Fig. 7 it is seen that the emulsion slicks in TSX2011a and TSX2012b show a large degree of overlap in all features. The feature values of TSX2011b differ more from the other two scenes, and are more similar to the different clean sea distributions. The wind conditions are quite similar in all three scenes, while slick ages and chemical properties vary. The very low incidence angle of TSX2011b may be one explanation for the difference between this scene and the other two.

Based on the features analysed in this paper, the phase information seem to be useful for slick detection and characterization, suggesting an advantage of the coherent imaging in TerraSAR-X compared to COSMO-SkyMed.

5   Conclusions and Further Work

An investigation of multi-polarization X-band SAR data for oil spill monitoring is here presented. Slicks of different types and ages are detected in low wind conditions (1.6-5 m/s) by both TerraSAR-X and COSMO-SkyMed over a range of incidence angles. Emulsion slicks as old as 34.5 hours are detected, and plant oil slicks (simulated look-alikes) as old as ~13 hours are imaged by both sensors.

Table 3 summarizes some of the findings for each scene in terms of noise contamination and visual contrast in multi-polarization features. Note that these findings are based on a limited data set. More comprehensive investigations on a larger database, including a range of weather conditions and slick types, are needed to draw general conclusions. The multi-polarization

features seem to be less useful at the lowest incidence angles, while noise contamination is a larger problem at higher incidence angles. Hence, medium range incidence angles seem to be preferred. For TerraSAR-X, incidence angles at least above 22° and well below 55° should be preferred based on the findings presented here. For COSMO-SkyMed, the scene with incidence angles ~23.5° – 26.1° is not useful for multi-polarization analysis, while the scenes of incidence angles > 39.6° are highly contaminated by noise. These findings may also be affected by other parameters such as oil properties and wind speed.

Intensity-based multi-polarization features gave poor results in terms of slick detection and characterization, with slightly better results in the normalized co-polarization difference compared to co-polarization power ratio. For TerraSAR-X, additional features, also utilizing the phase information are presented with more promising results. Especially at incidence angles ~27°-29° and ~ 41°-42°, slicks are clearly distinguished from surrounding sea, and consistency in feature values between scenes are seen to some extent. No clear variations with slick ages are observed in the features discussed here. Some visual difference between the simulated look-alike slick and the mineral oil slicks are observed in TerraSAR-X, but a relatively large degree of overlap is observed between feature distributions. Throughout the analysis, the three features including the phase information, i.e. the entropy, the real part of co-polarization correlation and the standard deviation of co-polarized phase difference give better results than the intensity-based features in terms of visual contrast and characterization potential. This suggests an advantage of the coherent imaging in TerraSAR-X compared to COSMO-SkyMed.

The further work on this data set will include a more thorough analysis of the multi-polarization features in terms of characterization potential. A quantitative investigation of feature values with respect to temporal change, and variations in slick ages and slick types will be applied. A normalization of the different features may be applied to improve the comparison among these. New SAR acquisitions are planned for the oil-on-water exercise in June 2013, and will be used to further evaluate the methods here investigated and improve the reliability of these results.

6   Acknowledgement

7   References

Brekke, C. and A. H. S. Solberg, "Oil Spill Detection by Satellite Remote Sensing", *Remote Sensing of Environment*, 95:1-13, 2005.

Cloude, S. R. and E. Pottier, "An Entropy Based Classification Scheme for Land Applications of Polarimetric SAR", *IEEE Trans. Geosci. Remote Sens.*, 35(1): 68 –78, 1997.

Danklmayer, A., B. J. Döring, M. Schwerdt and M. Chandra, "Assessment of Atmospheric Propagation Effects in SAR Images", *IEEE Trans. Geosci. Remote Sens.*, 47(10): 3507-3518, 2009.

Del Frate, F., A. Giacomini, D. Latini, D. Solimini and W. J. Emery, "The Gulf of Mexico Oil Rig Accident: Analysis by Different SAR Satellite Images", in *Proc. of SPIE Remote Sensing*, 8179, 2011.

Fritz, T. and M. Eineder, *TerraSAR-X Ground Segment Basic Product Specification Document*, DLR, 2010.

Gade, M., W. Alpers, H. Hühnerfuss, H. Masuko and T. Kobayashi, "Imaging of Biogenic and Anthropogenic Ocean Surface Films by the Multifrequency/Multipolarization SIR-C/X-SAR", *Journal of Geophysical Research*, 103(C9):18851-18866, 1998

Girard-Ardhuin, F., G. Mercier, F. Collard and R. Garello, "Operational Oil-Slick Characterization by SAR Imagery and Synergistic Data", *IEEE Journal of Oceanic Engineering*, 30(3): 487-495, 2005.

Hoogeboom, P. and L. Lidicky, "Introduction to Microwave Active Techniques and Backscatter Properties", in *Remote Sensing of the European Seas,* V. Barale and M. Gade (eds.), Springer Science+Business Media B.V., pp. 251-268, 2008.

Italian Space Agency, *COSMO-SkyMed SAR Products Handbook*, ASI, 2009.

Ivanov, A. YU., "The Oil Spill from a Shipwreck in Kerch Strait: Radar Monitoring and Numerical Modeling", *International Journal of Remote Sensing*, 31(17-18): 4853-4868, 2010.

Kim, D.-J., W. M. Moon and Y.-S. Kim, "Application of TerraSAR-X Data for Emergent Oil-Spill Monitoring", *IEEE Trans. Geosci. Remote Sens.*, 48(2): 852-863, 2010.

Migliaccio, M., A. Gambardella and M. Tranfaglia, "SAR Polarimetry to Observe Oil Spills", *IEEE Trans. Geosci. Remote Sens.,* 45(2): 506 –511, 2007.

Migliaccio, M., F. Nunziata, and A. Gambardella, "On the Co-Polarized Phase Difference for Oil Spill Observation", *Int. J. Remote Sens.*, 30(6): 1587–1602, 2009a.

Migliaccio, M., A. Gambardella, F. Nunziata, M. Shimada, and O. Isoguchi, "The PALSAR Polarimetric Mode for Sea Oil Slick Observation", *IEEE Trans. Geosci. Remote Sens.*, 47(12): 4032 –4041, 2009b.

Minchew, C. E. Jones, and B. Holt, "Polarimetric Analysis of Backscatter From the Deepwater Horizon Oil Spill Using L-Band Synthetic Aperture Radar", *IEEE Trans. Geosci. Remote Sens.*, 50(10): 3812–3830, 2012.

Minchew, B, "Determining the Mixing of Oil and Sea Water Using Polarimetric Synthetic Aperture Radar", *Geophysical Research Letters,* 39, 2012.

Nunziata, F., A. Gambardella, and M. Migliaccio, "On the Mueller Scattering Matrix for SAR Sea Oil Slick Observation", *IEEE Geosci. Remote Sens. Lett.*, 5(4): 691–695, 2008.

Nunziata, F. and M. Migliaccio, "On the COSMO-SkyMed PingPong Mode to Observe Metallic Targets at Sea", *IEEE Journal of Ocean Engineering*, 38(1): 71-79, 2013.

Skrunes, S., C. Brekke, and T. Eltoft, "A Comprehensive Analysis of Polarimetric Features for Oil Spill Characterization", in *Proc. SeaSAR*, Tromsø, Norway, 2012.

Tian, W., Y. Shao, J. Yuan, S. Wang, and Y. Liu, "An Experiment for Oil Spill Recognition Using RADARSAT-2 Image," in *Proc. IEEE Int. Geosci. Remote Sens. Symp.*, pp. 2761 –2764, 2010.

Velotto, D., M. Migliaccio, F. Nunziata, and S. Lehner, "Dual-Polarized TerraSAR-X Data for Oil-Spill Observation", *IEEE Trans. Geosci. Remote Sens.*, 49(12): 4751–4762, 2011.

Vespe, M., G. Ferraro, M. Posada, H. Greidanus, M. Perkovic, "Oil Spill Detection Using COSMO-SkyMed Over the Adriatic Sea: the Operational Potential", in *Proc. IEEE Int. Geosci. Remote Sens. Symp*, pp. 4403-4406, 2011

Zhang, B., W. Perrie, X. Li, and W. G. Pichel, "Mapping Sea Surface Oil Slicks Using RADARSAT-2 Quad-Polarization SAR Image", *Geophys. Res. Lett.*, 38(10), 2011.

Table 1 Data set overview. Wind speeds are based on the measurements from ships and platforms closest in time to satellite pass.

Image ID	Sensor	Date, time	Incidence angle	Slick types present	Wind speed
TSX2011a	TerraSAR-X	2011-06-08, 06.23	27.3° – 29.0°	Emulsion	1.6 – 3.3 m/s
TSX2011b	TerraSAR-X	2011-06-08, 17.11	19.9° – 21.7°	Plant oil, emulsion, crude oil	1.6 – 3.3 m/s
TSX2012a	TerraSAR-X	2012-06-14, 17.45	55.4° – 56.0°	No slicks visible	3 – 6 m/s
CSM2012a	COSMO-SkyMed	2012-06-14, 17.55	41.7° – 43.2°	Plant oil, emulsion	2 – 4 m/s
CSM2012b	COSMO-SkyMed	2012-06-15, 05.29	39.6° – 41.7°	Plant oil, emulsion	2 – 5 m/s
TSX2012b	TerraSAR-X	2012-06-15, 17.28	40.9° – 42.1°	Emulsion	2 – 4 m/s
CSM2012c	COSMO-SkyMed	2012-06-15, 19.01	23.5° – 26.1°	Emulsion	2 – 3 m/s
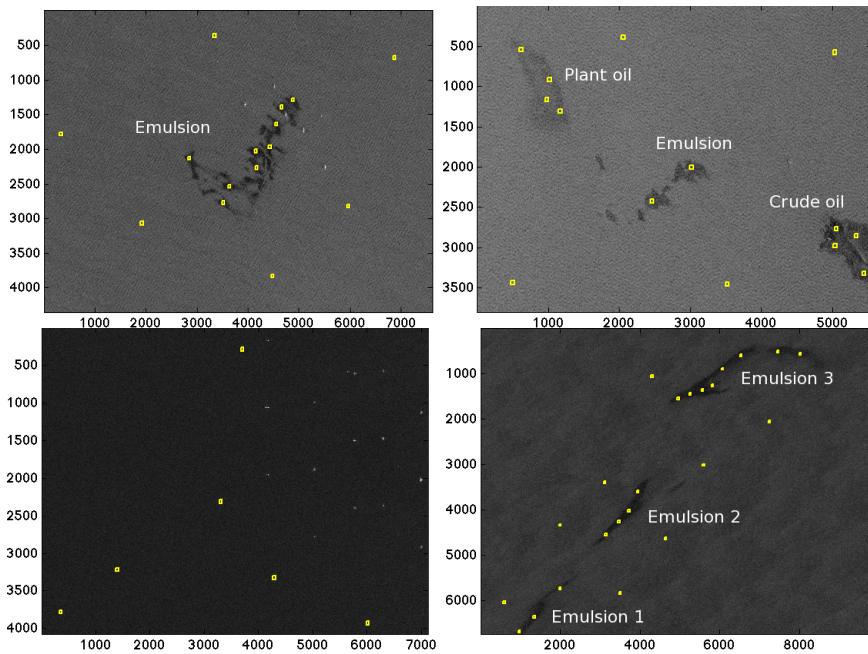
Figure 1 TerraSAR-X images, VV intensity. Clockwise from top left: TSX2011a, TSX2011b, TSX2012b and TSX2012a. The yellow boxes indicate selected areas used in the analysis. Copyright © 2011/2012 DLR
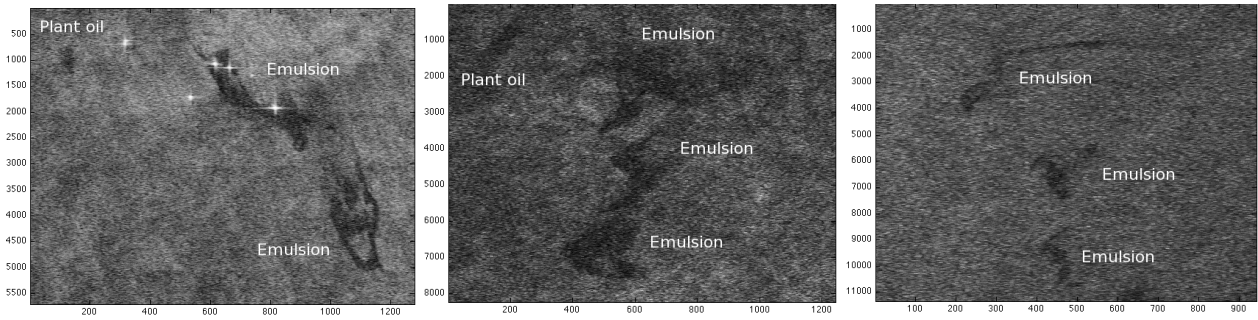
Figure 2 COSMO-SkyMed images, VV intensity. From left to right: CSM2012a, CSM2012b, CSM2012c. Copyright © ASI (2012)
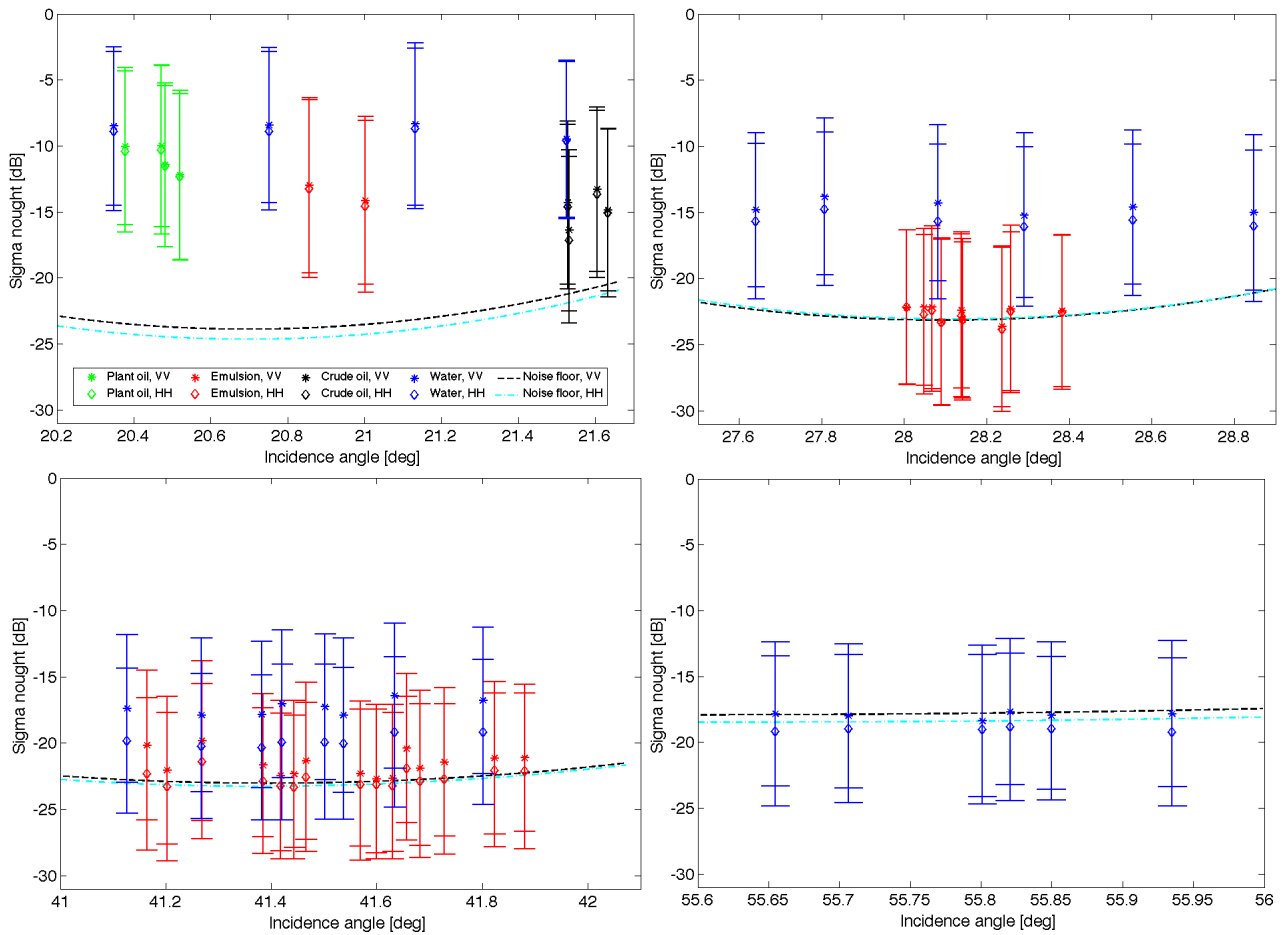
Figure 3 Signal-to-noise analysis of TerraSAR-X scenes. Clockwise from top left: TSX2011b, TSX2011a, TSX2012a, TSX2012b.

91

Table 2   Definitions of multi-polarization features.

Feature name	Definition	
Entropy	$$H' = -\sum_{i=1}^{2} p_i \, log_2 p_i$$	• $p_i = \lambda_i / (\lambda_1 + \lambda_2)$ • λ_i is the ith eigenvalue of the coherency matrix, $\lambda_1 > \lambda_2$
Real part of co-polarization correlation	$$r_{CO} = |\mathcal{R}(\langle S_{HH} S_{VV}^* \rangle)|$$	• $\mathcal{R}$ denotes the real part • $\langle \cdot \rangle$ denotes ensemble averaging • * is the complex conjugate • S_{HH} (S_{VV}) is the complex scattering coefficient in the HH (VV) channel
Standard deviation of co-polarized phase difference	$$\sigma_{\phi CO} = \sqrt{\langle(\phi_{HH} - \phi_{VV})^2\rangle - (\langle\phi_{HH} - \phi_{VV}\rangle)^2}$$	• ϕ_{HH} (ϕ_{VV}) is the phase of the complex scattering coeffient in the HH (VV) channel
Co-polarization power ratio	$$\gamma_{CO} = \frac{\langle|S_{HH}|^2\rangle}{\langle|S_{VV}|^2\rangle}$$	
Normalized co-polarization difference	$$D_{CO} = \frac{\langle|S_{VV}|^2\rangle - \langle|S_{HH}|^2\rangle}{\langle|S_{VV}|^2\rangle + \langle|S_{HH}|^2\rangle}$$	

*Co-polarization power ratio* *Normalized co-polarization difference*
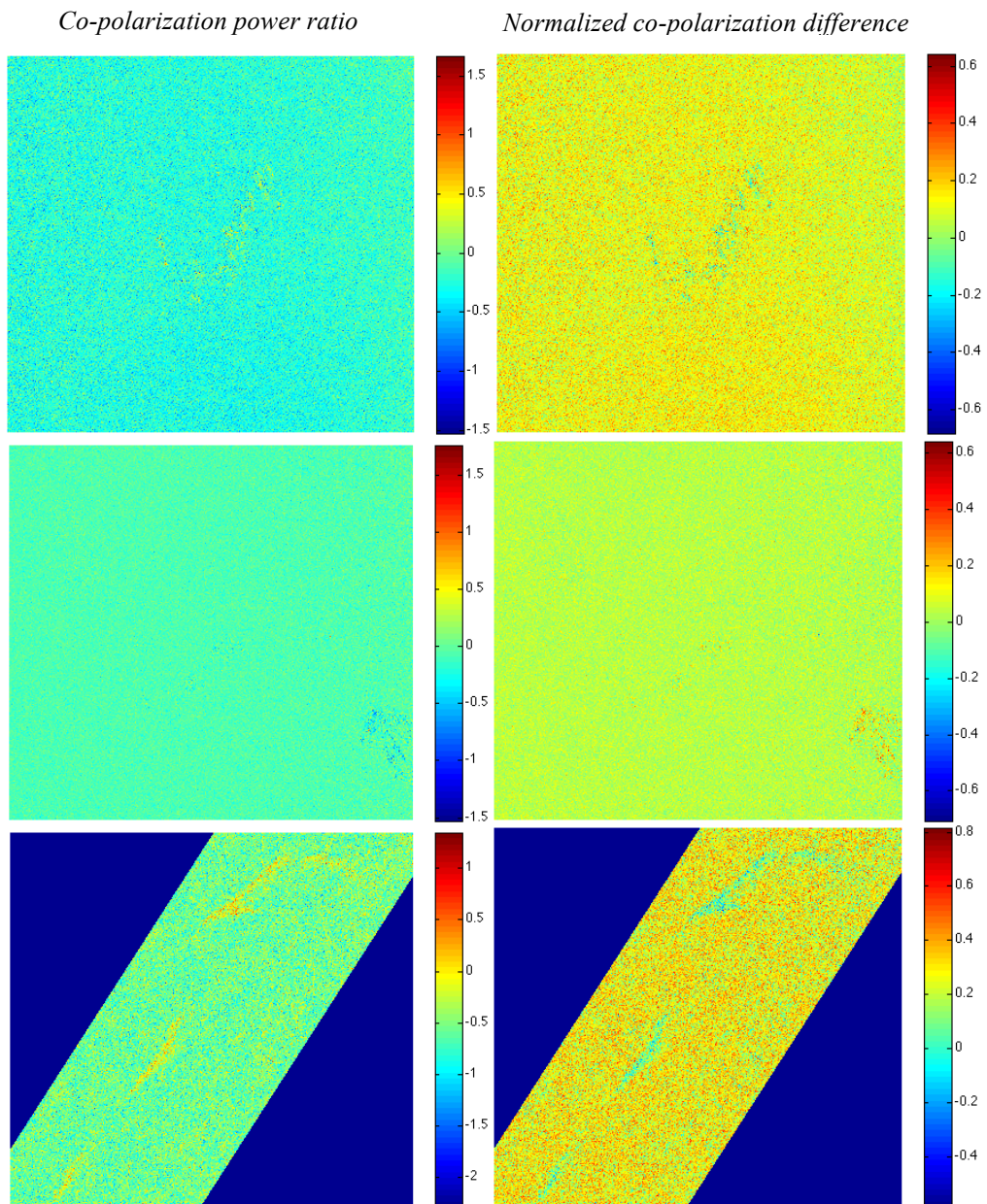
Figure 4 **Multi-polarization intensity based features. From top to bottom: TSX2011a, TSX2011b, TSX2012b. Co-polarization power ratio has been log transformed for all scenes.**

93
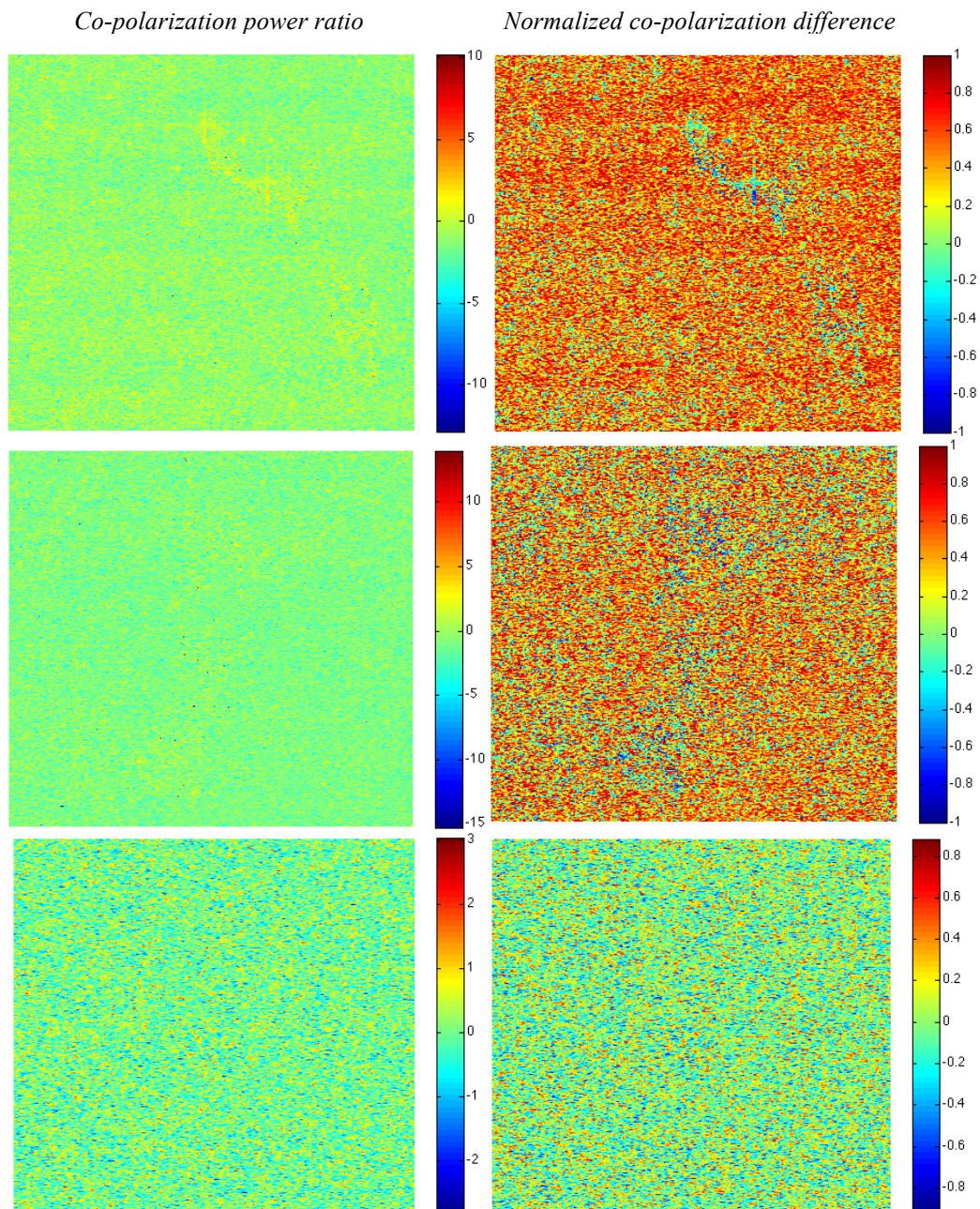
Figure 5   **Multi-polarization intensity based features. From top to bottom: CSM2012a, CSM2012b and CSM2012c. Co-polarization power ratio has been log transformed for all scenes.**

Entropy　　　　　　*Real part of co-pol correlation*　　　　　　*Std of co-pol phase difference*
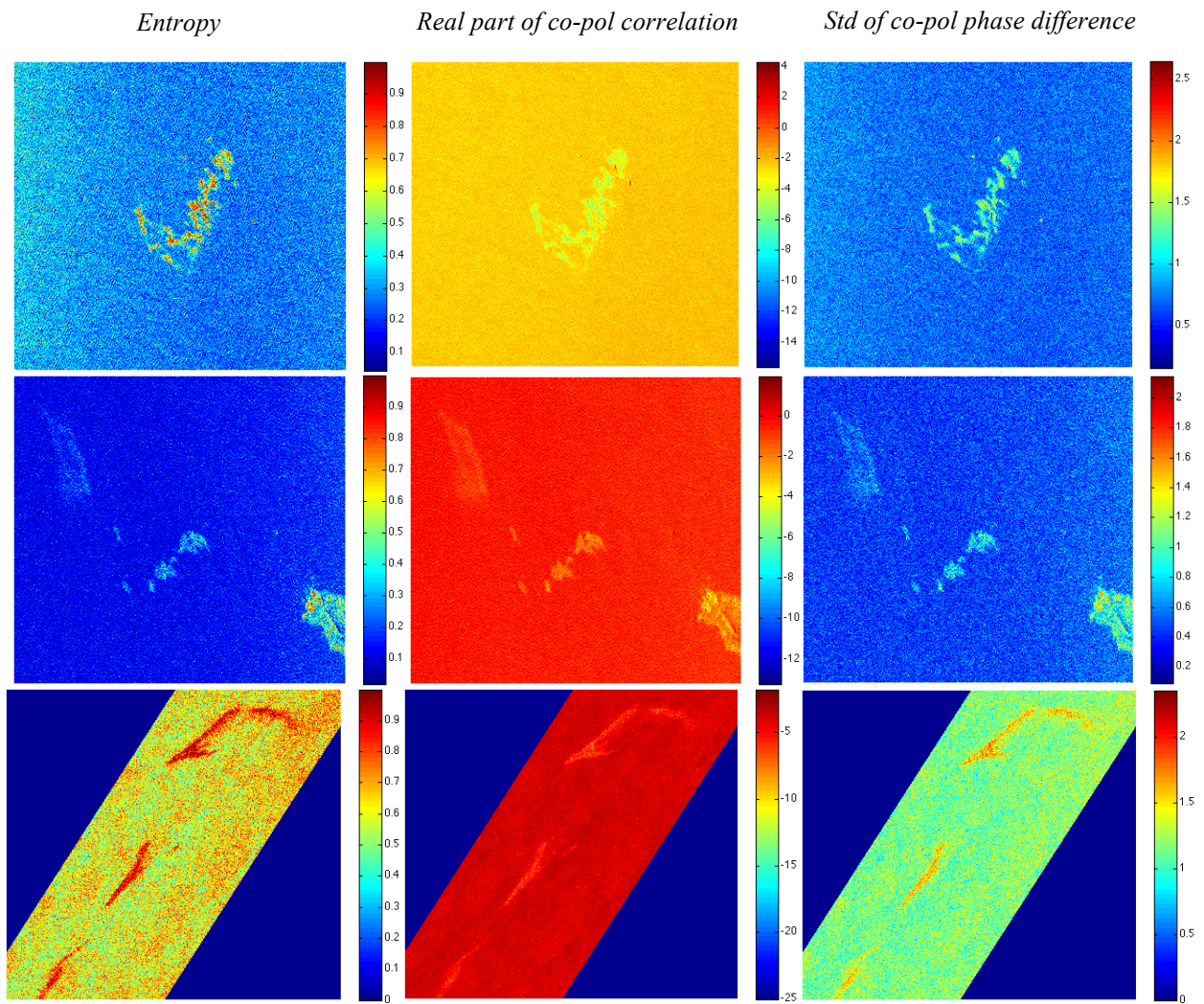
Figure 6　　　Multi-polarization features for TerraSAR-X scenes. From top to bottom: TSX2011a, TSX2011b, TSX2012b. Real part of co-polarization correlation has been log transformed for all scenes.
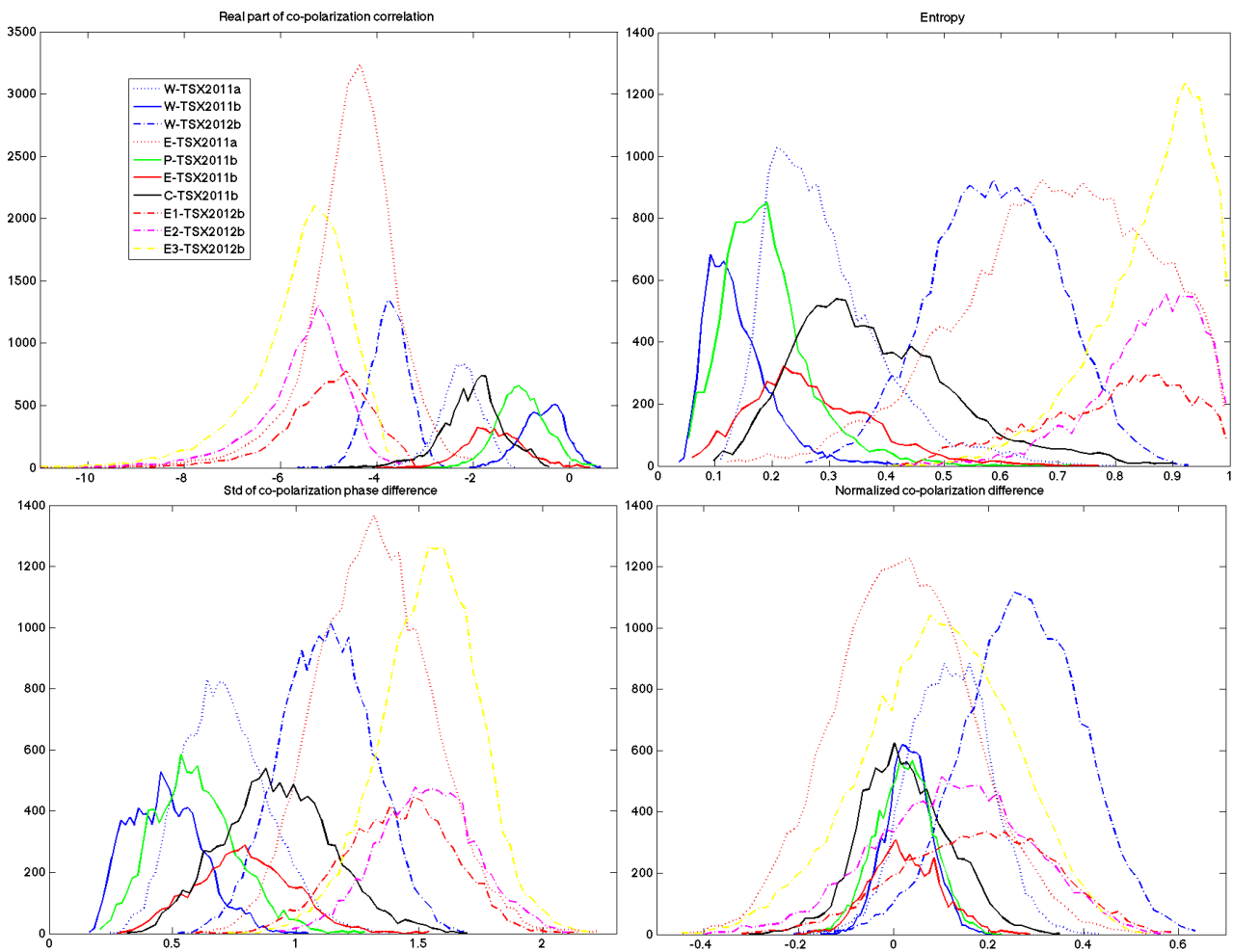
Figure 7 **Histograms of multi-polarization features based on selected regions in TerraSAR-X scenes. In the legend, "W" denotes water, "E" emulsion, "P" plant oil and "C" crude oil. "E1"-"E3" for TSX2012b denotes the different emulsion slicks.**

Table 3   Summary of some of the findings.

Image ID	Incidence angle	Noise contamination	Visual slick-to-sea contrast in features
TSX2011b	19.9° – 21.7°	Slick signal largely within one standard deviation of NESZ.	Slicks distinguishable from sea in features including phase information, but with low contrast, especially in plant oil slick.
TSX2011a	27.3° – 29.0°	Signal mean of slick regions close to or slightly below NESZ.	Slicks clearly distinguished from sea in features including phase information. Lower contrast in intensity based features.
TSX2012b	40.9° – 42.1°	Signal mean of slick regions close to NESZ. Signal mean of clean sea less than one standard deviation from NESZ.	Slicks clearly distinguished from sea in all features.
TSX2012a	55.4° – 56.0°	Signal mean of clean sea on or below NESZ.	Features not extracted, as slicks are not observed in this scene.
CSM2012c	23.5° – 26.1°	3.4% (HH and VV) zero due to noise.	No slicks discernible from sea.
CSM2012b	39.6° – 41.7°	71.1% (HH), 61.9% (VV) zero due to noise.	Mineral oil slick region can be identified, but results are noisy and boundaries unclear.
CSM2012a	41.7° – 43.2°	62.5% (HH), 49.4% (VV) zero due to noise.	Slick regions can barely be identified. Very noisy results.